Development of a sea-ice tank system for measuring microwave properties of sea ice

Masashige Nakayama[1], Kazuhiro Naoki[2], Tomonori Tanikawa[3] (iD) and Kohei Cho[2]

[1]Hokkaido University of Education, Kushiro Campus, Kushiro 085-8580, Japan; [2]Tokai University Research & Information Center, Tokyo 108-0074, Japan and [3]Meteorological Research Institute, Japan Meteorological Agency, Tsukuba 305-0052, Japan

Abstract

An outdoor sea-ice tank system for measuring the microwave properties of sea ice has been developed. With the natural cooling and the help of a cooling unit in the movable roof attached to the tank, the system can grow sea ice to about 50 cm thickness continuously without the effects of snowfall and/or melting. Portable microwave radiometers are attached beside the tank to measure the brightness temperature of the ice. As sea ice grows, the system can measure microwave brightness temperature, and seawater/ice temperature at each depth and thickness of sea ice. The bulk salinity of sea ice is measured by sampling. The following results were obtained from experiments conducted during two winters. (1) Rapid desalination was observed during the early stages of growth with ice thicknesses of 0–5 cm. (2) A new relational expression between ice thickness and bulk salinity at this thickness was obtained. (3) The rapid rise in microwave brightness temperature associated with the increase in sea-ice thickness during the early stages of sea-ice growth was captured in each frequency band. The microwave measurements from the sea-ice tank system are expected to provide new insights into the microwave properties of sea ice.

1. Introduction

The Intergovernmental Panel on Climate Change (IPCC) report says that the fluctuation of sea-ice extent covering the oceans in the North and South Polar Regions has been gaining attention under the serious situation of global warming (IPCC, 2021). Observations of global sea-ice extent from satellite-borne microwave radiometers have been performed since Electrically Scanning Microwave Radiometer (ESMR) onboard Nimbus-5 satellite in 1972 (Wilheit, 1972). Followed by Scanning Multichannel Microwave Radiometer (SMMR) onboard Nimbus-7 and Seasat-A satellites in 1978 (Njoku and others, 1980), Special Sensor Microwave/Imager (SSM/I) onboard DMSP satellite in 1987 (Hollinger and others, 1987), Advanced Microwave Scanning Radiometer (AMSR) onboard ADEOS-II satellite in 2002, Advanced Microwave Scanning Radiometer for EOS (AMSR-E) onboard Aqua satellite in 2002 (Kawanishi and others, 2003) and Advanced Microwave Scanning Radiometer 2 (AMSR2) onboard GCOM-W satellite in 2012 (Maeda and others, 2016). Sea-ice concentration can be estimated from brightness temperatures measured by the microwave radiometers. A number of methods have been proposed to estimate sea-ice concentration from those observed data (Ivanova and others, 2015). The estimated sea-ice concentration data derived from the time series observations of microwave radiometers onboard satellites are used for calculating the trend of global sea-ice extent. The results clarified the serious reduction of sea-ice extent in the Northern Hemisphere (Bjørgo and others, 1997; Comiso and Nishio, 2008; Comiso and others, 2008, 2017; Stroeve and others, 2012).

Ice thickness is another important sea-ice parameter to be estimated from satellite-borne microwave radiometers. Tateyama and others (2002) have studied the relationship between brightness temperature characteristics and the thickness using SSM/I. They showed that fast ice can be distinguished in seasonal sea-ice areas by using 85 GHz in addition to the conventionally used 19 and 37 GHz brightness temperatures. In addition, they proposed an empirical formula to determine ice thickness in seasonal sea-ice areas using SSM/I. Based on this method, Krishfield and others (2014) conducted applied research using the results of estimating ice thickness after dividing it into first-year-ice and older ice. Martin and others (2004) developed an algorithm that estimates sea-ice thickness up to 0.2 m in the Chukchi Sea, using 37 GHz brightness temperatures of SSM/I. Tamura and others (2007) proposed a method for estimating the thickness of thin ice that spreads over polynyas separately for the Southern Ocean and the Arctic Ocean using 37 and 85 GHz brightness temperatures of SSM/I. Kashiwase and others (2019) proposed a method to classify sea ice within polynyas into three types and estimate the thickness of each. Naoki and others (2008) have studied in detail the relationship between brightness temperature characteristics and the thickness and salinity of thin ice under synchronized aircraft and shipboard observations. Their results pointed out that the near-sea ice surface brine distribution is a key factor for detecting thin ice thickness with microwave radiometer. In the in situ experiment, a positive correlation between ice thickness <30 cm and brightness temperature was confirmed mainly at lower frequencies. In this way, attempts are being made to estimate sea-ice thickness using microwave radiometers.

cambridge.org/jog

Since the ground resolution of satellite microwave radiometers is from several kilometers to several tens of kilometers, the observed brightness temperature is the average value of the various sea ice coexisting within the field of view. It is difficult to continuously extract data on specific growth stage from satellite data. Although airborne observations have higher resolution than satellites, they are not suitable for continuously observing a specific area of sea ice. Therefore, in order to understand the basic microwave properties of sea ice, ground-based measurement is necessary. Since 1980s, microwave observations using outdoor tanks/pools have been conducted to investigate the microwave properties of thin ice (Arcone and others, 1986; Grenfell and Comiso, 1986; Swift and others, 1986; Nghiem and others, 1998; Shokr and others, 2009; Shokr and Kaleschke, 2012). Other related research using outdoor tanks/pools includes frost flower and oil spill experiments (Martin and others, 1995; Isleifson and others, 2014; Oggier and others, 2020; Asihene and others, 2022).

Grenfell and Comiso (1986) show that the microwave emissivity of thin ice increases with ice growth. The relationship with permittivity is discussed in detail by Germain and others (1993). The depth of the radiation source is wavelength-dependent and therefore different for each frequency band. Generally, the vertical salinity profile of thin ice is C-shaped. Naoki and others (2008) focused on the relationship between bulk salinity and brightness temperature in the surface layer of thin ice, thinking that the AMSR frequency band reflects the influence of the salinity of the surface layer. It has long been known that there is a tendency that near-surface salinity decreases with the total thickness as a result of brine drainage (Weeks and Lee, 1958). Naoki and others (2008) explained that when the surface salinity decreases, the dielectric properties change and the emissivity increases. As a result, they assumed that brightness temperatures would increase as surface salinity decreased.

We have performed several observations in Saroma-ko lagoon, Japan in winter, using a portable microwave radiometer. We have made a 2 m × 2 m hole in the frozen lake ice and measured the microwave brightness temperature of the growing lake ice. However, it was difficult to obtain the desired data (growth of sea ice due to freezing of seawater and associated changes in microwave brightness temperature) in a short period of time because Saroma-ko lagoon is easily affected by winter cyclones from the continent, and as a result, snowfall occurs frequently.

Thus, we have decided to develop an outdoor sea-ice tank for the measurement of the microwave properties of sea ice. The top of the tank is covered with a removable roof to control sea-ice growth and to avoid snow cover, and the roof can slide to open the top of the tank to be observed with microwave radiometers. In the roof, the refrigerator to cool the surface of seawater/ice is installed. The purpose of this paper is to report on the development and the performance of the new sea-ice tank system for measurement of the microwave properties of sea ice in detail. The whole view of a sea-ice tank system is explained in section 2. The results of experiments and discussion are described in section 3, and the conclusion is provided in section 4.

2. Instruments

2.1 System development strategy

In order to perform precise experiments on measuring microwave brightness temperature, salinity and thickness of sea ice, we have developed the sea-ice tank system emphasizing the following points. (1) Set up portable microwave radiometers which have the same observation frequency band and incident angle of the microwave radiometer currently in operation in space. (2) Design the size of the tank spacious enough to minimize the
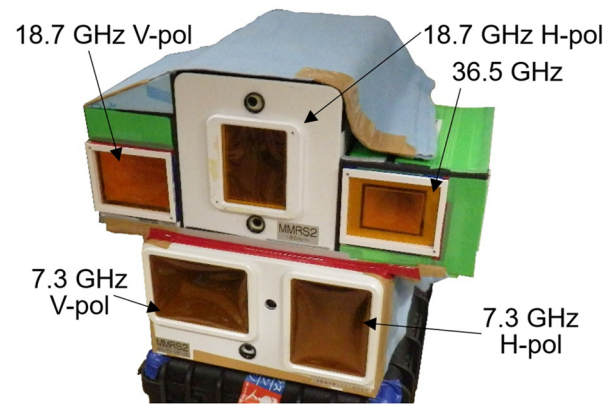
Figure 1. Outlook of the microwave radiometer MMRS2. Four portable radiometers were assembled into one. By wrapping the outer circumference with an electric blanket to keep it warm, it maintained stable operation even at low temperatures. The maximum dimensions of the entire radiometer are ~50 cm high × 60 cm wide × 50 cm deep.

microwave radiometer sidelobe effects and make sufficient space for sea-ice sampling without interfering with microwave radiometer observations. (3) Prevents sea ice from sticking to tank walls to maintain sea-ice freeboard. (4) Controls freezing/melting and snowfall to better understand brine movement in sea ice. (5) Obtain vertical temperature profiles to monitor sea-ice growth. (6) Design the entire system to be operated by one person to allow long-term data collection
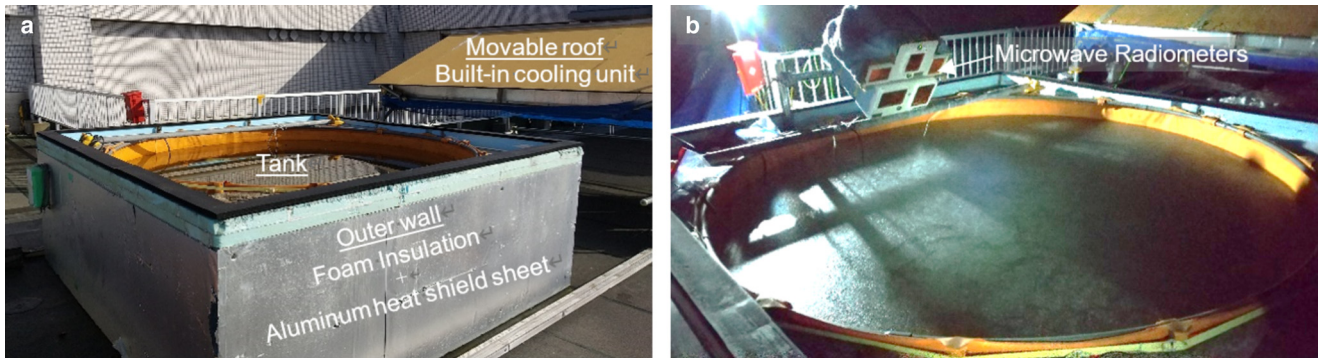
2.2 Microwave radiometer

Total of four portable microwave radiometer MMRS2 (Mitsubishi Electric Defense and Space Technologies Corporation, 1-15-9 Osaki, Shinagawa-ku, Tokyo 141-0032) was used in this study. The radiometers have an internal calibration function by the two-point calibration. A noise diode is used for the high-temperature reference source and a dummy load is used for the normal-temperature reference. In addition, before starting the experiment each year, we used a microwave absorber to check whether it was working properly. The radiometers consisted of a single-frequency instrument. The 7.3 GHz instrument has vertical and horizontal polarization channels. For the 18.7 GHz instruments, two were used for H and V polarization, respectively. As for 36.5 GHz, a single instrument was used and was rotated 90 degrees to perform V and H polarized observation. The instruments were set with the incident angle of 55 degrees to adjust with the incident angle of the microwave radiometer of AMSR2 onboard GCOM-W satellite (Kawanishi and others, 2003; Maeda and others, 2016). Figure 1 and Table 1 show the outlook and the specifications of the microwave radiometer MMRS2.

2.3 Sea-ice tank

Figures 2 and 3 show photographs and illustrations of the sea-ice tank with the microwave radiometer used in this study. The tank was installed on the roof of the seven-story building at Hokkaido

Table 1. Specifications of MMRS2

Parameter	Specification		
Center frequency	7.3 GHz	18.7 GHz	36.5 GHz
Polarization	V and H		Single (V or H)
Accuracy	1 K Typ.		
Beam width	15 degrees	10 degrees	7 degrees
Incident angle	55 degrees		

Figure 2. Photographs of the sea-ice tank. (a) Sea-ice tank before installing the microwave radiometer and (b) a scene of actual observation using the portable microwave radiometers at night.

University of Education Kushiro Campus (lat. 42°58′52″N, lon. 144°23′57″E, 40 m above sea level.). The front of the radiometer was clear of any obstructions that could cause unwanted noise.

In order to obtain the field of view of the portable microwave radiometer over the surface of seawater/ice, a round assembled tank (diameter 2.6 m, height 0.94 m) made of PVC sheets with reinforced fabric (National Marine Plastics Co., Ltd., Shinagawa, Tokyo, Japan) was employed as the sea-ice tank. The tank was setup outdoors to allow microwave radiometer observations. Seawater with a salinity of ∼32 psu, collected at a nearby fishing port, was stored in the tank for the experiment. In order to prevent cooling or warming from the side of the tank, the outer circumference of the tank was wrapped with 50 mm thick glass wool. Furthermore, the outer side and bottom of the tank was covered

Figure 3. Schematic illustration of the sea-ice tank with the microwave radiometers. (a) Top view of the tank. The field of view of the microwave radiometer is ∼60 cm square in the center of the tank. In advance, a metal plate was brought close to the periphery of the field of view to identify the area where sea-ice samples would not be affected. (b) Side view of the tank. The seawater surface is about 10 cm below the top of the tank. There is a PVC pipe frame at the top of the tank, and the outer circumference is fixed. The seawater surface was kept away from the pipe frame to avoid sea ice sticking.
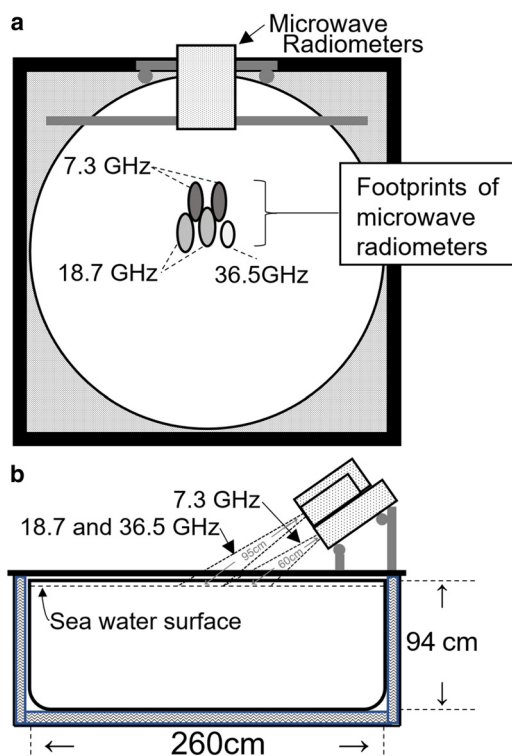
with a heat-insulating material (DuPont Styro Co., Ltd., Styrofoam EX, thickness 45 mm, Sanno Park Tower, 2-11-1 Nagatacho, Chiyoda-ku, Tokyo 100-6111) in a box shape.

Our tank was made of plastic-based materials with circular shape to prevent sea ice from freezing and sticking on the walls of the tank. As a result, the sea-ice freeboard can be represented inside the tank as sea ice grows. In our experiments, producing and maintaining the freeboard of sea ice is necessary because the concentration and distribution of brine in sea ice are important factors for microwave properties. In the preliminary experiment, it was confirmed that the sea-ice freeboard was always present. Various tank systems for laboratory sea-ice growth experiments were reviewed in detail by Hall and others (2023). Their review result also confirms the validity of our system design.

The tank was covered with a removable roof to avoid solar radiation and snowfall on the seawater/ice surface of the tank. The opening and closing of the roof were designed and built as the sliding roofs used in astronomical huts. A cooling unit was built into the hollow part of the roof for cooling the surface of the seawater/ice to speed up the freezing. The cooling unit is a ceiling-mounted integrated refrigeration unit (model: RU-N10LFV, Hitachi Global Life Solutions, Inc., Hitachi Atago Annex, 2-15-12 Nishi-Shinbashi, Minato-ku, Tokyo 105-8410). An elastic rubber sheet (10 mm thick) was pasted on the contact surface between the roof and the experimental tank section to make it airtight when the roof section was closed for cooling. Figure 4 shows the procedure for opening and closing the roof. The roof was separated from the lower tank by lifting a pillar to which four tires are attached. A hydraulic pant jack was used to lift the roof (Figs 4a, b). After lifting the roof by about 10 cm, the roof was moved along the tire rails on the ground (Fig. 4c) and then the microwave radiometer was set beside the tank (Fig. 4d). A series of these operations (including moving the roof) could be performed by one person and could be completed in about 30 min.
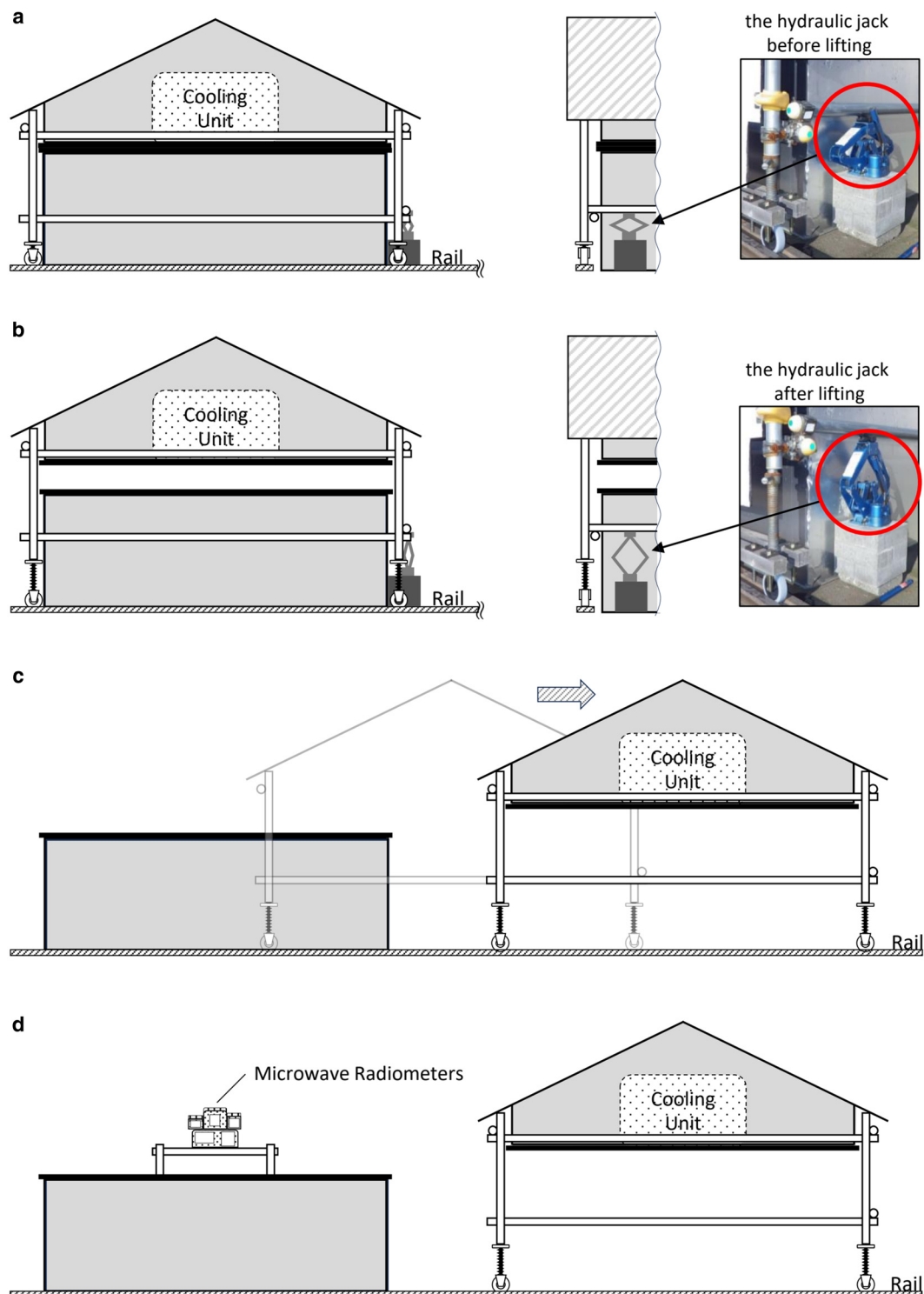
The optimal position of the radiometer was carefully examined. In order to secure the area to collect ice samples, we wanted to place the radiometer as close as possible to the ice surface to make the field of view size as small as possible. On the other hand, the radiometer should be placed far enough from the ice surface to avoid the effect of the antenna loading. Therefore, we started to measure the brightness temperature of the ice surface from 1.5 m distance and gradually shortened the distance. Finally, we placed the radiometer of 7.3 GHz at 60 cm, the radiometer of 18.7 GHz and 36.5 GHz at 95 cm far from the ice surface, which was far enough to avoid the effect of antenna loading and close enough to secure the area to collect ice samples (see Fig. 3).

In addition, several thermistors with data loggers were installed to continuously measure seawater and ice temperatures. Table 2 shows the specifications of the thermistor and data logger. As

Figure 4. Schematic illustration of the moving the roof and setting up the microwave radiometers. (a) The upper roof portion is in close contact with the lower tank portion. (b) The upper roof portion is lifted by hydraulic jacks. (c) The upper roof portion is moved. (d) Microwave radiometer system installed in the tank portion.

Table 2. Specifications of the thermistor and data logger

Thermistor	Measurement range	−60 to 155 °C
	Temperature durability	Ave. ±0.3 °C, at −20 to 80 °C
		Ave. ±0.5 °C, at −40 to −20 °C
	Response time (90%)	Approx. 90 s. (in air)
		Approx. 3 s. (in agitated water)
	Stainless tube (sensor)	SUS316, 70 mm, Φ 2.0 mm
Data logger	Measurement resolution	0.1 °C
	Recording interval	10 min

shown in Figure 5, it was installed in the seawater of the tank so that the vertical profile of temperature could be obtained. With the seawater surface at 0 cm, its probes were placed every 2.5 cm up to a depth of 10 cm and every 5 cm from a depth of 10 to 60 cm.

Sea-ice samples were collected to measure sea-ice thickness and bulk salinity. The salinity of the ice surface is also an important factor for detailed analysis of microwave radiation. However, since the experiment was conducted in a small ice tank, there was not enough space to do the sampling for both. Therefore, in this experiment, we decided to prioritize sampling to continuously measure the bulk salinity.
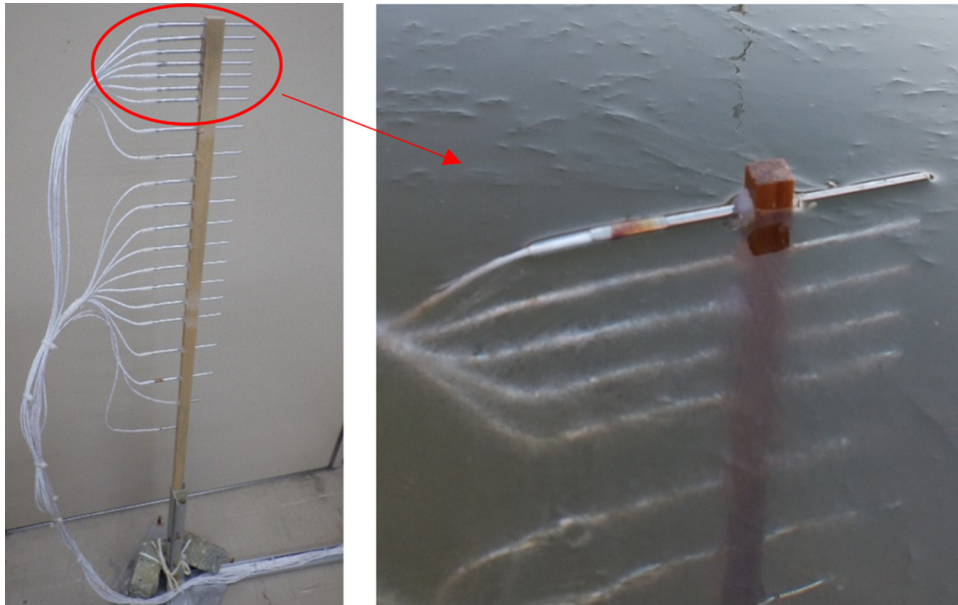
Figure 5. Thermistor for vertical profile measurement of seawater/ice temperature.

Ice sampling was performed by cutting the ice with a small keyhole saw. After making a square cut in the ice with the saw, the ice sample was lifted into a tray. After measuring the ice thickness, the sample in the tray was transferred to a plastic bag with the dripping brine. After the ice grew thicker than 40 cm, a core auger was used for ice sampling. Immediately after the core collection, it was cut into 3 cm thick pieces in 2019 and 5 cm thick pieces in 2020 to measure the salinity profile.

3. Results and discussion

3.1 Observation conditions

Experiments to grow ice from the open seawater surface in this tank were conducted in 2019 and 2020. The experiments were performed from 8 February to 8 March in 2019 and from 4 February to 16 March in 2020. Table 3 summarizes the conditions and maximum ice thickness observed for both years. The vertical profile of temperatures of sea ice was recorded using thermistors with data loggers at 10 min intervals (Fig. 5). The timing of measuring the microwave brightness temperature was matched with the ice growth. On the first day of the 2019 experiment, the lowest air temperature was −21.0 °C. The ice thickness reached 3.0 cm in 8 h from the start of the experiment. The lowest air temperature on the first day of the experiment in 2020 was −11.0 °C. The ice thickness reached 2.0 cm in 7 h from the start of the experiment. In both cases, the first day of the experiment was carried out at night when it was expected to be extremely cold. Since salinity and brightness temperature of sea ice rapidly change at the beginning of sea-ice formation, various measurements have to be taken at least every hour. From the second day onwards, and

until the ice thickness reaches ∼10 cm, measurements were taken every few hours to track the 1 cm increment of ice thickness. Thereafter, since the change speed of thickness, salinity and brightness temperature of ice slowdown, measurements were taken at intervals of ∼5–10 days. At each measurement, ice samples were taken after the microwave radiometer measurements. The samples were melted to measure bulk salinity. Measurements were taken at intervals of several days after the ice thickness exceeded ∼15 cm. In all cases, measurements were carried out from night to early morning to avoid melting of the sea-ice surface caused by solar radiation. Brine in liquid phase can be released onto the ice surface. Therefore, we carefully observed whether brine has seeped onto the surface at each time we opened the roof. However, no such condition was confirmed.

3.2 Temperature changes of each depth of ice due to ice growth

Figure 6 shows the changes in temperature of ice at each depth and ice thickness during the experiment. In Figure 6, a total of five sharp valley-shaped temperature reduction can be observed for the data of 0 cm depth ('↑' in the figure), which is shown between the start of the experiment to the 5th or 6th day. This was recorded when the air temperature dropped to around −10 to −20 °C at night. This experiment at the initial stage of sea-ice growth was carried out during the period when the night-time air temperature was lower. At that time, the cooling unit attached on the roof was not used at night, and the upper part of the tank was opened to allow ice to grow by natural cooling. During other

Table 3. Observation conditions and maximum ice thickness in both years

Date and time the cooling started	Feb. 8, 2019 / 23:30	Feb. 4, 2020 / 20:00
Cooling experiment end date	Mar. 8, 2019 / 04:32	Mar. 16, 2020 / 03:10
Number of days observed (day)	27.2	40.3
Seawater salinity at the start of the experiment (psu)	32.0	32.5
Set temperature of cooling unit (°C)	−15	−10/−15*/−20**
Maximum ice thickness (cm)	48.5	54.5

Time indicates a local time (JST).
*After the ice thickness was 29.5 cm, the cooling temperature was set to −15 °C.
**After the ice thickness was 45.0 cm, the cooling temperature was set to −20 °C.
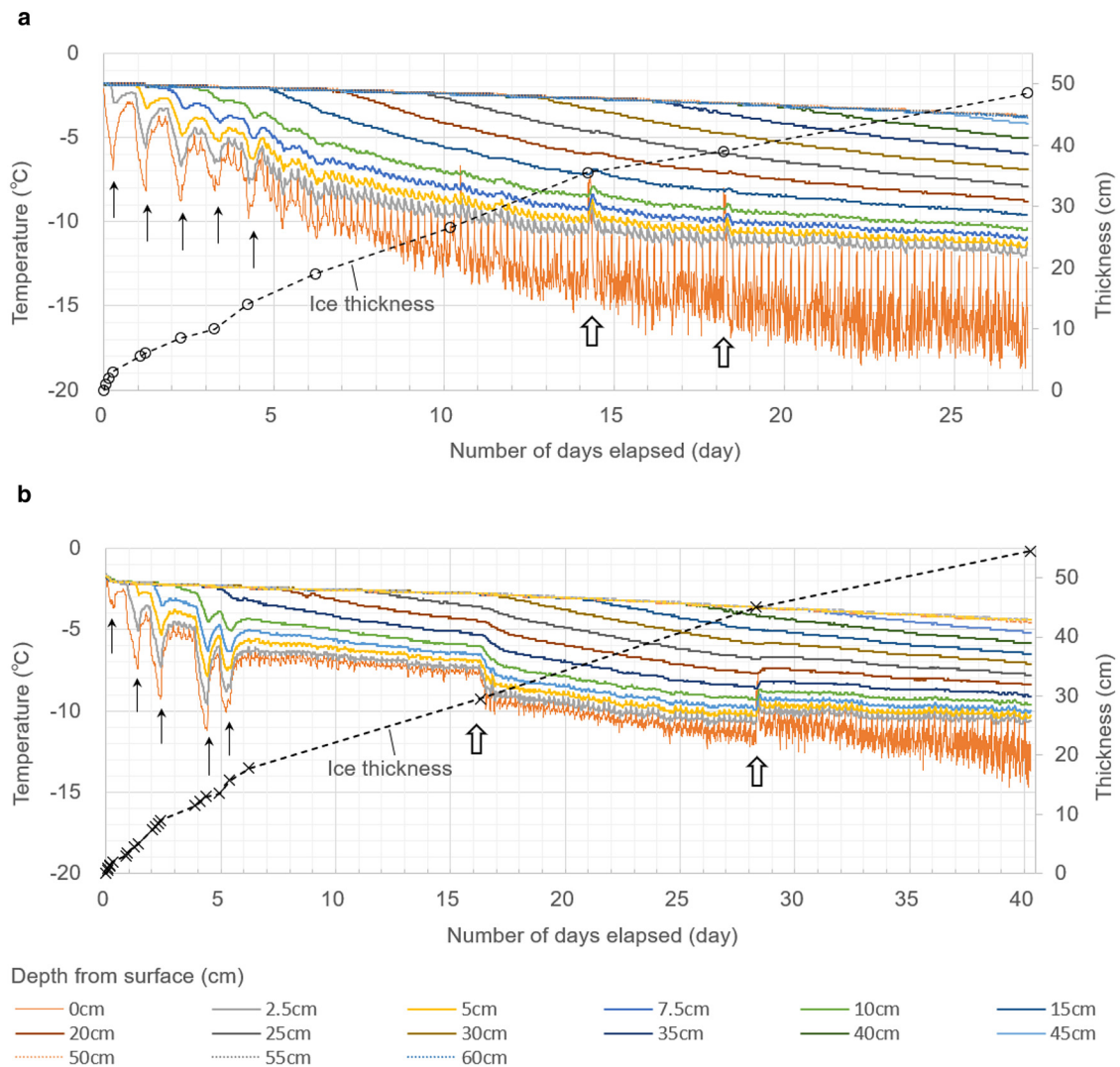
Figure 6. Ice, seawater temperature and ice thickness during the evolution of open water to ice. (a) Experiment results in 2019. (b) Experiment results in 2020.

periods when the temperature at 0 cm depth spikes 4–5 times in a day, the tank was covered with the roof and the cooling unit was used. Only when the cooling unit was in use, this repeated spike in temperature rise was recorded. This was caused by the activation of the defrosting function of the cooling system, which occurred approximately every 5 h.

The temperature change at 0 cm depth in 2019 shows a temperature increase of 5–6 °C on the 14th and 18th days (see '⇧' in Fig. 6a). Those are the days when the collection of ice pillars was carried out. Since the roof was open for a while during the work, the temperature of the ice surface increased.

Looking at the temperature change of 0 cm depth in 2020, a gap can be confirmed on the 16th and 28th days (see '⇧' in Fig. 6b). These gaps correspond to the time of opening and closing of the roof between the measurement of microwave brightness temperature and ice thickness. Since the temperature of the surface layer has started to decrease from the 16th day, the effect of setting the cooling unit to low temperature is apparent. The temperature of the surface layer slightly increased on the 28th day due to the failure of the cooling unit.

3.3 Thickness versus bulk salinity of ice

Ice samples were taken immediately after measuring the microwave brightness temperature during the experiment and melted

for bulk salinity measurements. Figures 7a and c show that the bulk salinity of ice is a function of ice thickness. A similar trend was observed in the decrease of ice bulk salinity with ice growth in the two experiments. This bulk salinity behavior of sea ice supports the fact that brine in the sea ice was discharged as the sea ice grew. In addition, the bulk salinity profile of the ice is shown in Figures 7b and d. To examine the vertical distribution of bulk salinity in detail, ice cores were collected on the 5th day and final day in the 2019 experiment. In the 2020 experiment, it was collected only on the final day. From Figure 7b, the salinity profile is similar to the C-shape on the 5th day after the start of the experiment. At the end of the experiment, it was confirmed that as the sea ice grows, the overall temperature of the ice decreases, the brine becomes more concentrated and flows down, and the salinity of all layers decreases. As a result, the seawater of high salinity existed in water column of the tank. From Figure 7d, it can be confirmed that it becomes the same profile at the end of the 2020 experiment.

The relationship between ice thickness and bulk salinity measured is shown in Figure 8 together with that by the Cox and Weeks model (Cox and Weeks, 1974). Our experiment captured a rapid change in bulk salinity in the very early growth stage (a few centimeters thick) of sea ice (corresponding to *Dark Nilas* (WMO, 2014)). Notz and Worster (2008) found that salinity discharge is about twice as high in the first few hours after that when
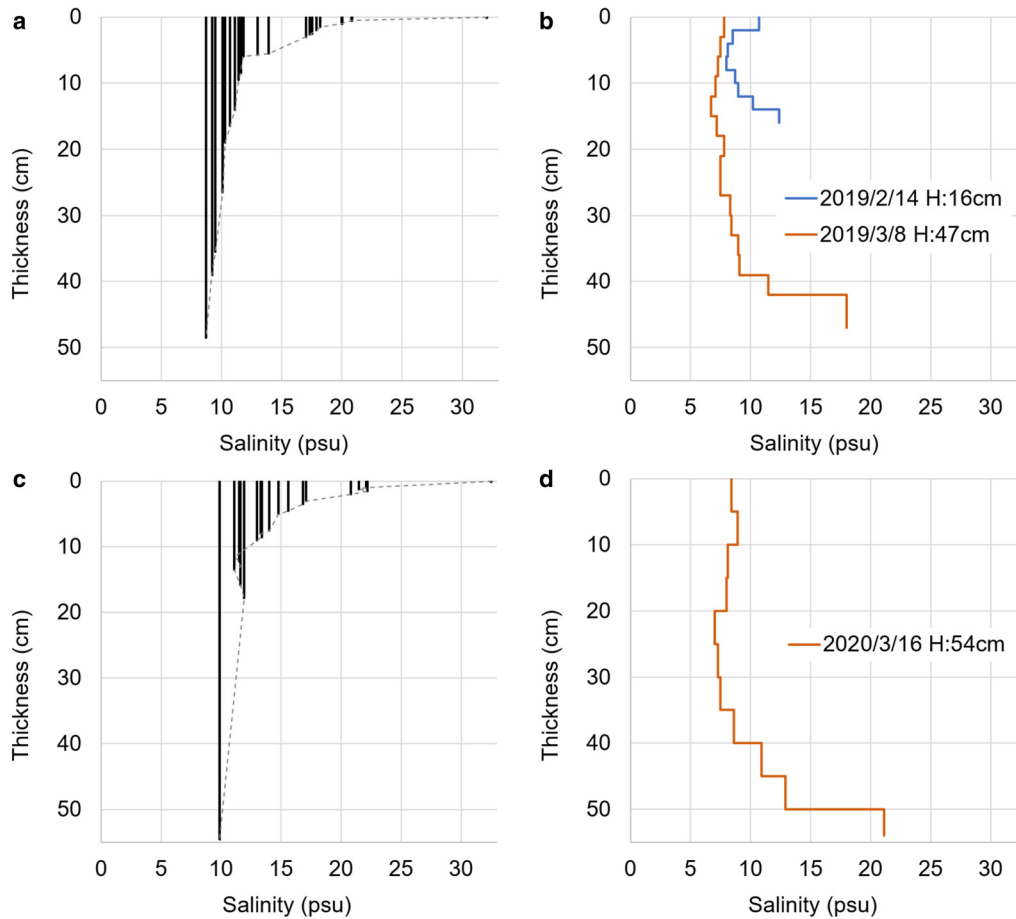
Figure 7. Bulk salinity of ice as a function of ice thickness and bulk salinity profile of ice core samples. (a) Thickness versus whole bulk salinity of ice during experiment in 2019. (b) Bulk salinity profile of two ice cores with thickness at 5 days from the start of the experiment and at the end of the experiment in 2019. (c) Thickness vs whole bulk salinity of ice during experiment in 2020. (d) Bulk salinity profile of ice core with thickness at the end of the experiment in 2020.

new sea ice forms from the surface in 1×1 m hole made in landfast ice. The similar results were obtained in this tank experiment. Comparing the observation results of this experiment with the model of Cox and Weeks (1974), it can be seen that the ice thicknesses agree in the range of 5–20 cm (Fig. 8). On the other hand, the model does not match with our experiment result of the ice thickness range of 0–5 cm. In their model, empirical equations were obtained using observed values for ice thicknesses of 8 cm or more. In Figure 8, it is clear that the relationship between ice thickness and bulk salinity dramatically changes at ice thickness of ~5 cm. Thus, we considered that for ice thicknesses of 5 cm

or less, new regression equations were needed for ice thickness and bulk salinity. The relationship between ice thickness below 5 cm and bulk salinity is given by,

$$S = 22.35 - 160h \tag{1}$$

where h is the ice thickness (m) and S is the bulk salinity (psu).

In summary, using the range of standard errors of 1.5 psu with Cox and Weeks (1974) with ice thicknesses of 40 cm or less as one criterion, the bulk salinity of the ice obtained in this experiment was found to be comparable to that of naturally grown sea ice
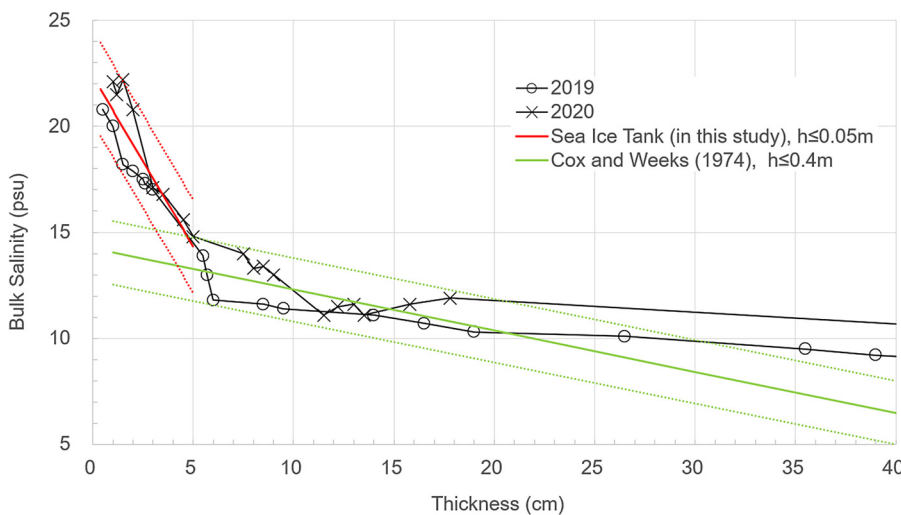
Figure 8. Relationship between bulk salinity of ice and ice thickness, and results calculated by Cox and Weeks (1974). The Cox and Weeks models showed with a range of 1.5 psu standard error. A new model with an ice thickness of less than 5 cm was added based on the observation data obtained in this study. The new models showed with a range of 2.2 psu standard error. Standard error ranges are indicated by dashed lines, respectively.
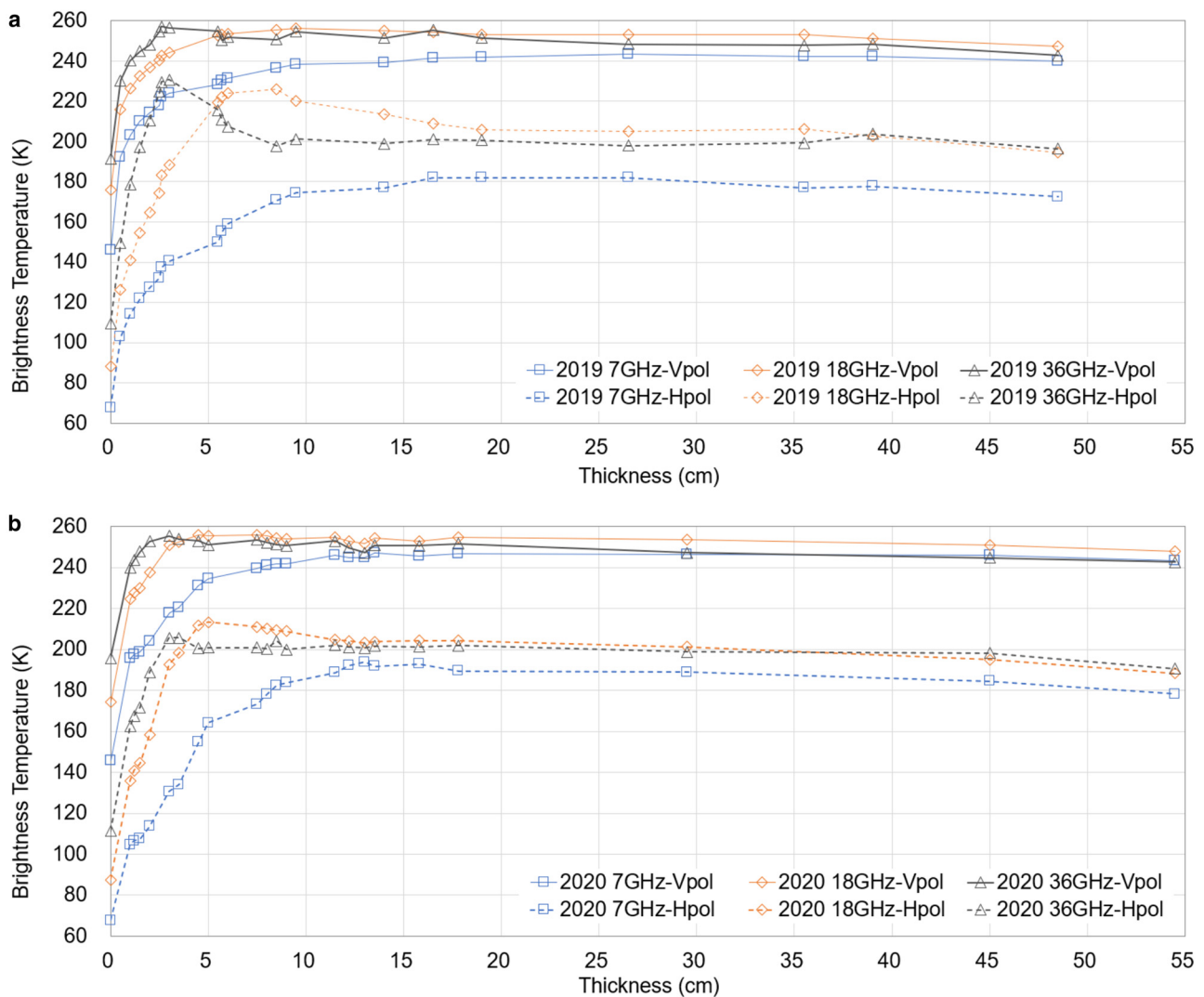
Figure 9. Brightness temperature for different frequencies and horizontal/vertical polarizations versus ice thickness. (a) Experiment results in 2019 and (b) experiment results in 2020.

for ice thicknesses of 5–20 cm. However, for ice thicknesses of 5 cm or less, a rapid decrease in salinity with ice growth was observed in this experiment, indicating that the conventional approach by the Cox and Weeks model is not applicable.

3.4 Microwave brightness temperature

The results of the microwave brightness temperature measurements are shown in Figure 9, together with ice thickness. The brightness temperature values are the observed values. Observations were conducted late at night under clear skies to avoid the effects of downwelling atmospheric radiation as much as possible. It is possible that there is a small amount of downwelling atmospheric radiation reflected from the water surface. However, since the effect is smaller at the ice surface compared to the water surface (Shokr and others, 2009), the authors considered that the effect is negligible. Grenfell and Comiso (1986) reported from the result of a pool experiment that the brightness temperature changes as the surface roughness changes. They pointed out that this is especially noticeable when the roughness scale and the wavelength of the frequency band are close. In our experiment, since the still sea water was cooled and began to freeze in a quiet environment, the surface of the sea ice was smooth and flat from the beginning. Additionally, by covering the ice tank with a roof for cooling except during observation,

the surface was not disturbed by snowfall or sunlight. As a result, the experiment was successfully conducted without the influence of surface roughness.

In both the 2019 and 2020 experiments, the brightness temperature increased in the early stages of ice growth, from the open seawater surface to the ice as its thickness increased. Furthermore, it was observed that the order in which the brightness temperature reached its maximum value depends on the frequency. This occurs for both vertical and horizontal polarization. Mills and Heygster (2011) state by model simulation: 'What these results show is a modest and fairly rapid increase in emissivity with thickness as the ice becomes progressively more opaque, thus less of the water shows through'. This situation was captured in this experiment.

After recording the maximum value of brightness temperature, it was confirmed that the brightness temperature decreased as the ice thickness increased. However, the values converged to almost constant when the ice thickness exceeded 15 cm. This decrease in brightness temperature was more pronounced for horizontally polarized waves than for vertically polarized waves. For example, in 2019, it is 4 K at 7.3 GHz, 9 K at 18.7 GHz, 15 K at 36.5 GHz in vertical polarization, and 10 K at 7.3 GHz, 32 K at 18.7 GHz, 35 K at 36.5 GHz in horizontal polarization, respectively.

By using the sea-ice tank we developed, simultaneous observations were made in the 7.3 GHz, 18.7 GHz and 36.5 GHz frequency bands while allowing the sea ice to grow without changing the

sample, and brightness temperature data up to ~50 cm ice thickness could be obtained without being affected by snow accumulation or melting due to solar radiation on the sea-ice surface.

4. Conclusions and discussion

In this paper, we have presented the results of the development of a field sea-ice tank system for measuring microwave brightness temperature, thickness, temperature and salinity of sea ice. Natural seawater is stored in a tank surrounded by insulation. It has a roof with a built-in cooling unit. This system enables observation with a microwave radiometer while controlling the growth of sea ice. Using this tank, sea ice was continuously grown from the open water surface to a thickness of ~50 cm without the effects of snowfall and melting while maintaining sea-ice freeboard. The changes in its microwave brightness temperature were successfully observed. Measurements were also made on the salinity and thickness of sea ice, which are necessary to understand the changes in microwave brightness temperature of sea ice in the early stages of growth. As a result, the ice thickness up to ~20 cm was equivalent to that of sea ice grown in the natural calm sea even though the experiment was conducted in a tank space on land. Especially in this range, we succeeded in capturing the relationship between the ice thickness and frequency-dependent brightness temperature in detail. The result strongly suggested that certain limitation exists in estimating sea-ice thickness from microwave observation. Additionally, a new equation of the relationship between ice thickness and bulk salinity was obtained for ice thicknesses of 5 cm or less.

Pancake ice can also be made in this tank by circulating seawater. The next step of our study is to produce various types of sea ice by simulating various grow processes of natural sea ice using this sea-ice tank system. At that time, it is necessary to add a function to adjust the salinity of the seawater, which is increased by the discharged salt water as sea ice grows, when the thick ice is the object of the experiment. The data obtained from this sea-ice tank system will provide important information for understanding the microwave brightness temperature properties of sea ice.

References

Arcone SA, Gow AJ and McGrew S (1986) Microwave dielectric, structural, and salinity properties of simulated sea ice. *IEEE Transactions on Geoscience and Remote Sensing* GE-24(6), 832–839.

Asihene E and 10 others (2022) Toward the detection of oil spills in newly formed sea ice using C-band multipolarization radar. *IEEE Transactions on Geoscience and Remote Sensing* 60, 4302615. doi: 10.1109/TGRS.2021.3123908

Bjørgo E, Johannessen OM and Miles MW (1997) Analysis of merged SMMR–SSMI time series of Arctic and Antarctic sea ice parameters 1978–1995. *Geophysical Research Letters* 24(4), 413–416.

Comiso JC and Nishio F (2008) Trends in the sea ice cover using enhanced and compatible AMSR-E, SSM/I, and SMMR data. *Journal of Geophysical Research: Oceans* 113, C02S07.

Comiso JC, Parkinson CL, Gersten R and Stock L (2008) Accelerated decline in the Arctic sea ice cover. *Geophysical Research Letters* 35, L01703.

Comiso JC, Meier WN and Gersten R (2017) Variability and trends in the Arctic sea ice cover: results from different techniques. *Journal of Geophysical Research: Oceans* 122, 6883–6900. doi: 10.1002/2017JC012768

Cox GFN and Weeks WF (1974) Salinity variations in sea ice. *Journal of Glaciology* 13(67), 109–120.

Germain KM, Swift CT and Grenfell TC (1993) Determination of dielectric constant of young sea ice using microwave spectral radiometry. *Journal of Geophysical Research: Oceans* 98(C3), 4675–4679. doi: 10.1029/92JC02755

Grenfell TC and Comiso JC (1986) Multifrequency passive microwave observations of first-year sea ice grown in a tank. *IEEE Transactions on Geoscience and Remote Sensing* GE-24(6), 826–831.

Hall B, Johnson S, Thomas M and Rampai T (2023) Review of the design considerations for the laboratory growth of sea ice. *Journal of Glaciology* 69, 953–965. doi: 10.1017/jog.2022.115

Hollinger J, Lo R, Poe G, Savage R and Peirce J (1987) *Special Sensor Microwave/Imager User's Guide.* Washington, D. C.: U.S. Naval Research Laboratory, 119pp.

Intergovernmental Panel on Climate Change (IPCC) (2021) Climate change 2021: the physical science basis. Contribution of Working Group I to the Sixth Assessment Report of the Intergovernmental Panel on Climate Change. Cambridge University Press, Cambridge, United Kingdom and New York, NY, USA, 2391 pp. doi: 10.1017/9781009157896

Isleifson D and 5 others (2014) A study on the C-band polarimetric scattering and physical characteristics of frost flowers on experimental Sea Ice. *IEEE Transactions on Geoscience and Remote Sensing* 52(3), 1787–1798. doi: 10.1109/TGRS.2013.2255060

Ivanova N and 10 others (2015) Inter-comparison and evaluation of sea ice algorithms: towards further identification of challenges and optimal approach using passive microwave observations. *The Cryosphere* 9(5), 1797–1817. doi: 10.5194/tc-9-1797-2015

Kashiwase H, Ohshima KI, Fukamachi Y, Nihashi S and Tamura T (2019) Evaluation of AMSR-E thin ice thickness algorithm from a mooring-based observation: how can the satellite observe a sea ice field with nonuniform thickness distribution? *Journal of Atmospheric and Oceanic Technology* 36, 1623–1641. doi: 10.1175/JTECH-D-18-0218.1

Kawanishi T and 9 others (2003) The Advanced Microwave Scanning Radiometer for the Earth Observing System (AMSR-E), NASDA's contribution to the EOS for global energy and water cycle studies. *IEEE Transactions on Geoscience and Remote Sensing* 41(2), 184–194.

Krishfield RA and 7 others (2014) Deterioration of perennial sea ice in the Beaufort Gyre from 2003 to 2012 and its impact on the oceanic freshwater cycle. *Journal of Geophysical Research: Oceans* 119(2), 1271–1305. doi: 10.1002/2013JC008999

Maeda T, Taniguchi Y and Imaoka K (2016) GCOM-W1 AMSR2 level 1R product: dataset of brightness temperature modified using the antenna pattern matching technique. *IEEE Transactions on Geoscience and Remote Sensing* 54(2), 770–782.

Martin S, Drucker R and Fort M (1995) A laboratory study of frost flower growth on the surface of young sea ice. *Journal of Geophysical Research: Oceans* 100(C4), 7027–7036. doi: 10.1029/94JC03243

Martin S, Drucker R, Kwok R and Holt B (2004) Estimation of the thin ice thickness and heat flux for the Chukchi Sea Alaskan coast polynya from Special Sensor Microwave/Imager data, 1990–2001. *Journal of Geophysical Research: Oceans* 109, 1–15. doi: 10.1029/2004JC002428

Mills P and Heygster G (2011) Sea ice brightness temperature as a function of ice thickness: computed curves for AMSR-E and SMOS (frequencies from 1.4 to 89 GHz). Technical Report DFG project HE-1746-15. doi: 10.48550/arXiv.1202.3802

Naoki K and 5 others (2008) Thin sea ice thickness as inferred from passive microwave and in situ observations. *Journal of Geophysical Research: Oceans* 113(C02S16), 1–11.

Nghiem SV and 7 others (1998) Diurnal thermal cycling effects on microwave signatures of thin sea ice. *IEEE Transactions on Geoscience and Remote Sensing* 36(1), 111–124.

Njoku EG, Stacey JM and Barath FT (1980) The Seasat scanning multichannel microwave radiometer (SMMR): instrument description and performance. *IEEE Journal of Oceanic Engineering* OE-5(2), 100–115. doi: 10.1109/JOE.1980.1145458

Notz D and Worster M (2008) In situ measurements of the evolution of young sea ice. *Journal of Geophysical Research: Oceans* 113, 1–7. doi: 10.1029/2007JC004333

Oggier M, Eicken H, Wilkinson J, Petrich C and O'Sadnick M (2020) Crude oil migration in sea-ice: laboratory studies of constraints on oil mobilization and seasonal evolution. *Cold Regions Science and Technology* 174, 102924, ISSN 0165-232X. doi: 10.1016/j.coldregions.2019.102924

Shokr M and Kaleschke L (2012) Impact of surface conditions on thin sea ice concentration estimate from passive microwave observations. *Remote Sensing of Environment* 121, 36–50.

Shokr M, Asmus K and Agnew TA (2009) Microwave emission observations from artificial thin sea ice: the Ice-tank experiment. *IEEE Transactions on Geoscience and Remote Sensing* **47**(1), 325–338.

Stroeve JC and 5 others (2012) The Arctic's rapidly shrinking sea ice cover: a research synthesis. *Climatic Change* **110**, 1005–1027.

Swift CT, Dehority DC, Tanner AB and Mcintosh RE (1986) Passive microwave spectral emission from saline ice at C-band during the growth phase. *IEEE Transactions on Geoscience and Remote Sensing* GE-24(6), 840–848.

Tamura T and 5 others (2007) Estimation of thin ice thickness and detection of fast ice from SSM/I data in the Antarctic ocean. *Journal of Atmospheric and Oceanic Technology* **24**(10), 1757–1772. dio: 10.1175/jtech2113.1

Tateyama K, Enomoto H, Toyota T and Uto S (2002) Sea ice thickness estimated from passive microwave radiometers. *Polar Meteorology and Glaciology* **16**, 15–31.

Weeks WF and Lee OS (1958) Observations on the physical properties of sea-ice at Hopedale, Labrador. *Arctic* **11**(3), 134–155. doi: 10.14430/arctic3740

Wilheit TT (1972) The Electrically Scanned Microwave Radiometer (ESMR) experiment. Nimbus-5 User's Guide, NASA Goddard Space Flight Center, Greenbelt, Maryland, 59-105.

World Meteorological Organization (WMO) (2014) Sea Ice Nomenclature. WMO, 259, 121pp.